RESEARCH PAPER

A Novel Surfactant Synthesis of BaTi0.85Zr0.15O3 (BTZ): Highly Efficient Catalyst for Synthesis of 1,5-benzodiazepine Derivatives under Solvent-free Conditions

Elham Amouhadi, Razieh Fazaeli, Hamid Aliyan *

Department of Chemistry, Shahreza Branch, Islamic Azad University, 86145-311, Iran

ARTICLE INFO

ABSTRACT

The main objective of this research is to develop efficient and environmentally benign heterogeneous catalysts for synthesis of 1,5-benzodiazepine derivatives. For this purpose, for the first time, heterogeneous $BaTi_{0.85}Zr_{0.15}O_3$ (BTZ) catalyst was prepared by hydrothermal synthesis in the presence of hexadecylamine (HAD) as surfactant, followed by solvothermal method, and the prepared catalyst was characterized by various techniques such as X-ray diffraction (XRD), scanning electron microscopy (SEM), N_2 adsorption-desorption, Fourier-transform infrared (FTIR), Thermogravimetric (TG-DTG) and Temperature programmed desorption (NH_3-TPD) analysis. BTZ is easily used as a heterogonous, reusable and efficient catalyst for synthesis of 1,5-benzodiazepine by reaction of o-phenylenediamine with different ketones under various conditions. The advantages of this catalytic system is mild reaction conditions, short reaction times, high product yields, easy preparation of the catalysts, non-toxicity of the catalysts, simple and clean work-up of the desired products. Furthermore, the solid catalyst demonstrates long durability for synthesis of 1,5-benzodiazepine derivatives consecutively for at least four cycles under mild conditions.

INTRODUCTION

Due to pharmacological and industrial properties, benzodiazepines and their polycyclic derivatives are very significant compounds [1]. Particularly, 1,5-benzodiazepines are useful precursors for the synthesis of some fused ring benzodiazepine derivatives, such as triaxolo-, triazolo-, oxadiazolo-, oxazino- or furano-benzodiazepines [2]. Many reagents have been reported in the literature for the synthesis of benzodiazepine including AlTP and AlMP [3], $H_3PMo_{12}O_{40}$ [4], boric acid [5], Clay (KSF and K10)-supported heteropoly acids [6], glycerol [7] and BF_3–H_2O [8]. However, many of these methodologies are associated with several shortcomings, such as long reaction times, low yields, drastic reaction conditions, co-occurrence of several side products and very expensive reagents. Moreover, the main disadvantage of the reported methods is that the catalysts are destroyed in the work-up procedure and cannot be recovered or reused.

Metal oxide nanomaterials represent a growing asset in many industries, especially with their heightened chemical, physical, and electronic properties compared with their bulk counterparts. Metal oxide nanomaterials are versatile materials that can be used in applications such as environmental remediation, medical

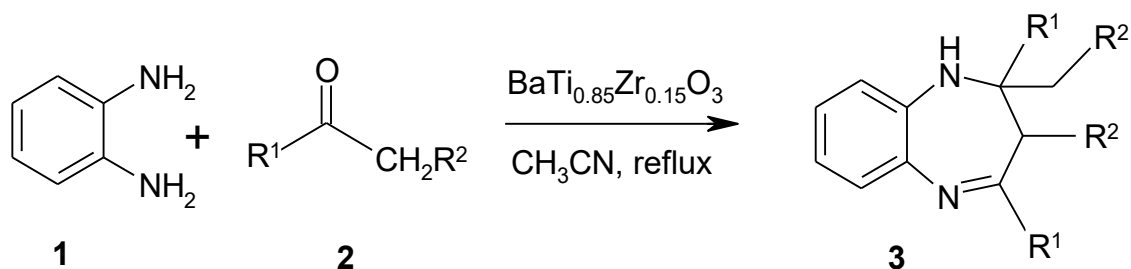* *Corresponding Author Email: aliyan@iaush.ac.ir*

Fig. 1. Proposed mechanism for the synthesis of 1,5-benzodiazepine derivatives by $BaTi_{0.85}Zr_{0.15}O_3$ (BTZ).

technology, energy, water treatment, and personal care products [9-13]. Barium titanate ($BaTiO_3$) is a perovskite type (ABO_3) ferroelectric material that has been known since the 1940s [14] However, it still attracts much attention as a promising and environmentally friendly material for a variety of electronic devices such as capacitors, memory storage systems, piezoelectric, pyroelectric and microwave components [15,16]. Among the possible modifications, the substitution of Ti^{+4} ion by the larger ionic radius Zr^{+4} in the B-site leads to the solid solution compound $BaTi_{1-x}Zr_xO_3$ (BTZ_x) [17].

Herein, we wish to report a suitable method for the use of $BaTi_{0.85}Zr_{0.15}O_3$ (BTZ) as heterogeneous catalysts for the synthesis of 1,5-benzodiazepine derivatives (Fig. 1).

MATERIALS AND METHODS
Chemicals and Instruments

Hexadecylamine 98% (HAD), Titanium(IV) isopropoxide 97% and zirconium butoxide was purchased from Sigma-Aldrich; chemicals. All other reagents were of analytical grade and used without treatment.

A Perkin Elmer Spectrum 65 spectrophotometer was applied to record infrared spectra (400–4000 cm^{-1}) from KBr pellets. Cu Kα (1.54056 Å) radiation with automatic control was employed to gain powder XRD diffraction patterns on a XRD, Bruker D8 ADVANCE and PW1830 instrument. Adsorption/desorption of nitrogen at liquid nitrogen temperature was operated to determine BET specific surface areas and pore volumes of the catalysts with a Micromeritics BELSORT mini II instrument. The samples were outgassed at 623 K for 12h under a vacuum of 10^{-4} Pa prior to the adsorption measurements. Catalyst pore sizes were achieved from the peak positions of the distribution curves detected by the adsorption branches of the isotherms. In temperature programmed desorption of ammonia (NH_3-TPD; Nano sort-NS91), 0.1 g of the catalyst was taken in a U-shaped, flow-through, quartz sample tube. Thermogravimetric analysis (TG) and differential thermal analysis (DTA) were carried out on a BAHR-STA-504 apparatus. Thermal analyses were utilized in the range of 25 °C-800 °C, with a heating rate of 10 $K.min^{-1}$.

Preparation of $BaTi_{0.85}Zr_{0.15}O_3$ (BTZ)

$BaTiO_3$ (0.8 g) was homogeneously dispersed in ethanol (97.4 mL) by ultrasonication, followed by the addition of 1.0 g of hexadecylamine (HAD), as surfactant, and 2 mL of ammonia, and stirring at room temperature for 30 min to form a uniform dispersion. Then, 1.1 mL of titanium isopropoxide and 1.7 mL of zirconium butoxide was added to the dispersion under stirring; the milky white mixture was kept static after 2 h 5 and then aged at room temperature overnight. The white powder sol was collected by centrifugation then washed with water and ethanol several times. To prepare hollow mesoporous BTZ nano spheres with Cubic framework, a solvothermal treatment of the precursor beads was performed. A 1.6 g of the BTZ precursor spheres was dispersed in a 20 mL ethanol and 10 mL water mixture with an ammonia concentration of 0.5 M. Then the resulting mixtures were sealed within a Teflon-lined autoclave (50 mL) and heated at 160 °C for 16 h. After centrifugation and ethanol washing, the air-dried powders were calcined at 600 °C for 4 h in air to remove HDA templates for characterization. The experimental procedure is presented in the flowcharts of Fig. 2.

General procedure for synthesis of 1,5-benzodiazepine derivatives in solution

The reactions were carried out by taking a 1:2.5 mole ratio mixture of 1,2-phenylenediamine and the ketone in the presence of catalytic amount of

```
┌──────────┐  ┌──────────────────────┐  ┌──────────┐
│  BaTiO₃  │  │ Hexadecylamine (HAD) │  │ Ammonia  │
└──────────┘  └──────────────────────┘  └──────────┘
                         │
              ┌─────────────────────┐
              │   Stirring at r.t.  │
              └─────────────────────┘
                         │
   ┌───────────────────────────────────────────────┐
   │ Titanium Isopropoxide + Zirconium butoxide     │
   └───────────────────────────────────────────────┘
                         │
              ┌─────────────────────┐
              │    Aged at r.t.     │
              └─────────────────────┘
                         │
              ┌─────────────────────┐
              │ Teflon-line autoclave│
              └─────────────────────┘
                         │
              ┌─────────────────────┐
              │  Dried and Calcined │
              └─────────────────────┘
```
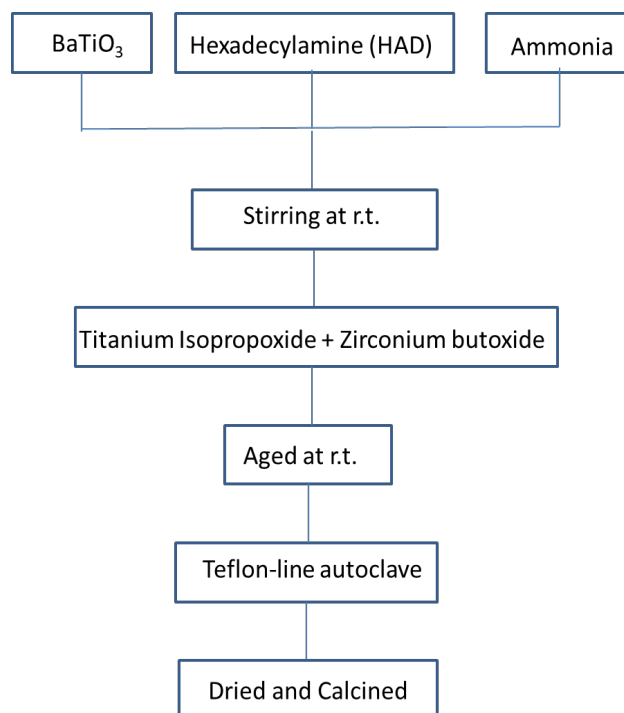
Fig. 2. Flow chart to BTZ powder preparation.

BTZ nano spheres (0.1 g) in a mortar with a pestle at room temperature for the appropriate time. The progress of the reaction was monitored by GC. After completion of the reaction, 10 ml of CH_2Cl_2 was added to the reaction mixture and the catalyst was recovered by filtration. The organic layer was concentrated and the products was purified by silica gel column (100–200 mesh) and eluted with EtOAc:n-hexane (2:8) to afford pure compound in 80–98% yield. The wet catalyst was recycled and no appreciable change in activity was noticed after a few cycles. The spectral data of the some of the compounds are given below.

RESULTS AND DISSCUSSION

Characterization

Fig. 3 presents the FT-IR spectrum of BTZ nano spheres with an absorption region of 400–4000 cm^{-1}. Several bands were observed for BTZ nano spheres in the FT-IR spectrum. It is well known that two kinds of OH- groups, such as a surface adsorbed OH- and a lattice OH- group can be observed in bariumtitanate [18]. The broad low-intensity peak with the maximum around 3407 cm^{-1} has been assigned to O-H stretching modes of surface adsorbed water corresponding to the stretching vibrations of weakly bound water interacting with its environment via hydrogen bonding and to stretching vibrations of hydrogen-bonded OH groups. The 1618 cm^{-1} peak was due to the deformation mode of absorbed H_2O molecules, assigned to the bending vibration. FTIR for pure BTZ sample shows that a strong peak around 596 cm^{-1} appeared, which was assigned to TiO_6 stretching vibration that connected to the barium ion and Ti-O stretching vibration along the polar axis of spontaneous polarization in BTZ with tetragonal phase like $BaTiO_3$ [19,20].

Fig. 4 displayed showed the XRD pattern of $BaTi_{0.85}Zr_{0.15}O_3$, and the diffraction peaks of $BaTi_{0.85}Zr_{0.15}O_3$ corresponded well in position with the standard pattern, indicating the phase purity of the sample. The strong peaks (2q) included 22.63, 31.97, 39.33, 45.68, 51.33, 56.63, 66.13, 70.78, and 75.48, which corresponded to (010), (011), (111), (020), (102), (112), (022), (212), and (130) crystal planes, based on JCPDS card No. 74-1963. The sample showed good crystallinity. The crystallite size of the calcined powder was determined as 12 nm from the full-width half maximum (FWHM) of the (111) crystallographic plane using Scherrer's relation [21], with a rhombohedral structure [22].

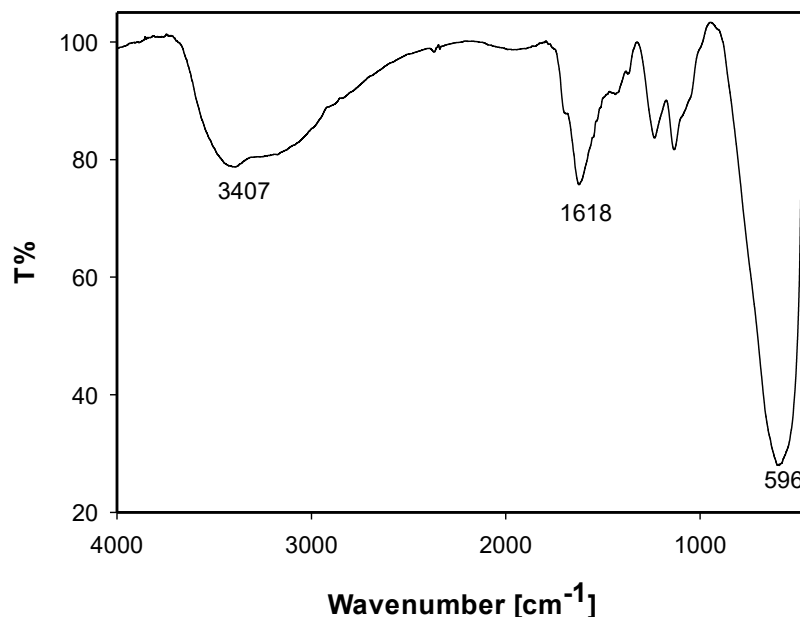The interplanar distance (d) and the crystallite size (D) of the as-prepared sample are estimated

Fig. 3. FTIR spectra of BTZ nano spheres.

using the Bragg (1) and the Scherrer formula (2), respectively [23]:

$$n\lambda = 2d\,sin\theta \tag{1}$$

$$D = \frac{k\lambda}{(\beta cos\theta)} \tag{2}$$

Where n is a positive integer, λ is the wavelength of the Cu Kα radiation (λ = 0.15406 nm), k = 0.89

(the Scherrer constant), β is the width of the peak (full width at half maximum (FWHM)), and θ is the diffraction angle. The average interplanar distance and crystallite size of the sample estimated using the Bragg and the Scherrer formula from its XRD patterns are ~0.2044 nm and ~18.61 nm, respectively.

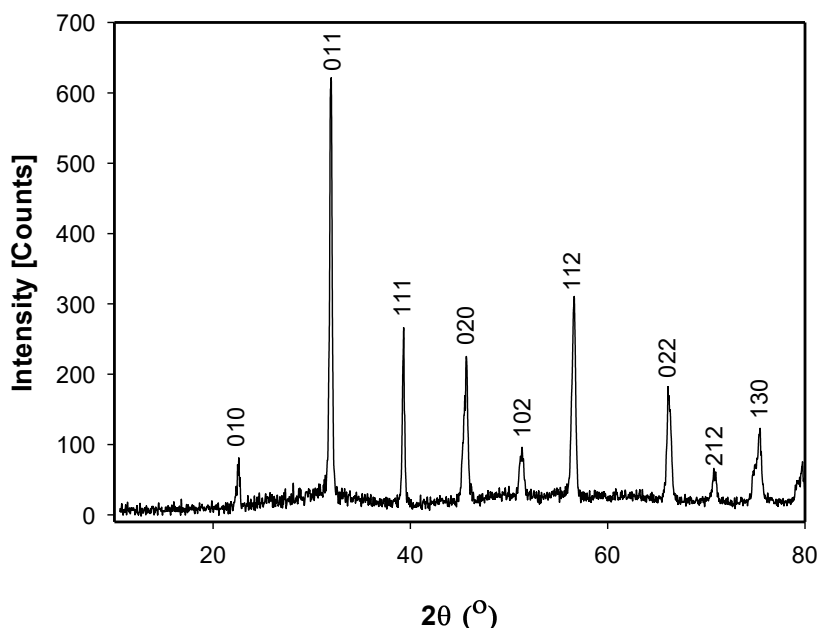The dislocation density (δ) and strain (ε) are calculated using equations (3,4) [24]. The

Fig. 4. XRD patterns of BTZ.

Table 1. The structural parameters of multiphase (BTZ).

2θ (°)	hkl	FWHM (β) °C	Crystallite size (D) (nm)	d-Spacing (nm)	Dislocation density (δ) ×10⁻³ nm⁻²	Strain (ε) ×10⁻⁴
22.6250	010	0.3810	21.0305	0.3925	2.2610	3.3239
31.9750	011	0.3170	25.7825	0.2796	1.5044	3.9609
39.3250	111	0.2866	29.1118	0.2288	1.1799	4.4660
45.6750	020	0.4600	18.5331	0.1984	2.9114	8.4484
51.3250	102	0.6564	13.2796	0.1778	5.6706	1.3754
56.6250	112	0.4857	18.3746	0.1624	2.9619	1.1411
66.1250	022	0.5396	17.3739	0.1411	3.3129	1.5319
70.7750	212	0.7417	12.9937	0.1330	5.9229	2.2977
75.4750	130	0.9016	11.0195	0.1258	8.2353	3.0431

calculated crystallite size and other structural parameters are shown in Table 1.

$$\text{Dislocation density } (\delta) \ = \ \frac{1}{D^2} \qquad (3)$$

$$\text{Strain } (\varepsilon) \ = \ \beta_{hkl}/(4tan\theta) \qquad (4)$$

According to Williamson-Hall (W-H) equation (5) [25], a plot is drawn with 4sinq along the x-axis and bcosq along the y-axis for as-prepared BTZ as shown in Fig. 3.

$$\beta_{hkl}cos\theta = \frac{k\lambda}{D} + 4\varepsilon sin\theta \qquad (5)$$

From the linear fit to the data, the crystalline size was estimated from the y-intercept, and the strain e, from the slope of the fit. Equation represents the UDM (Uniform Deformation Model), where the strain was assumed to be uniform in all crystallography directions, thus
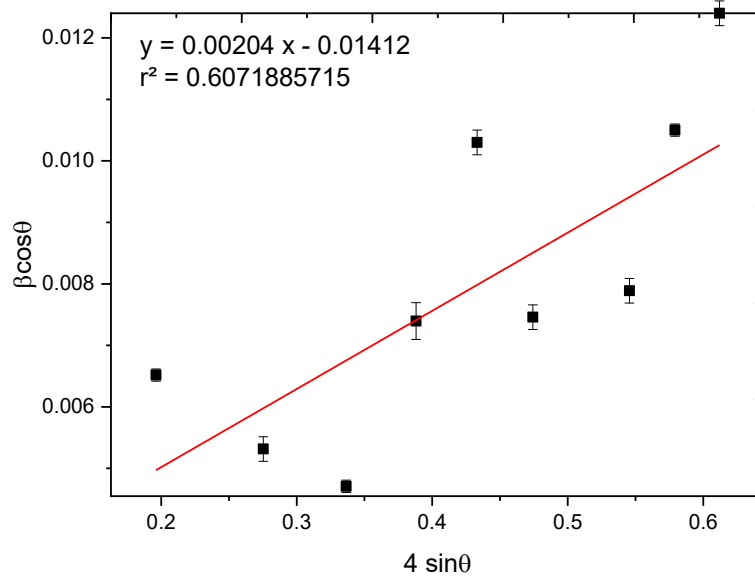

y = 0.00204 x - 0.01412
r² = 0.6071885715

Fig. 5. The W-H analysis of BTZ assuming UDM. Fit to the data, the strain is extracted from the slope and the crystalinity size is extracted from the y-intercepte of the fit.
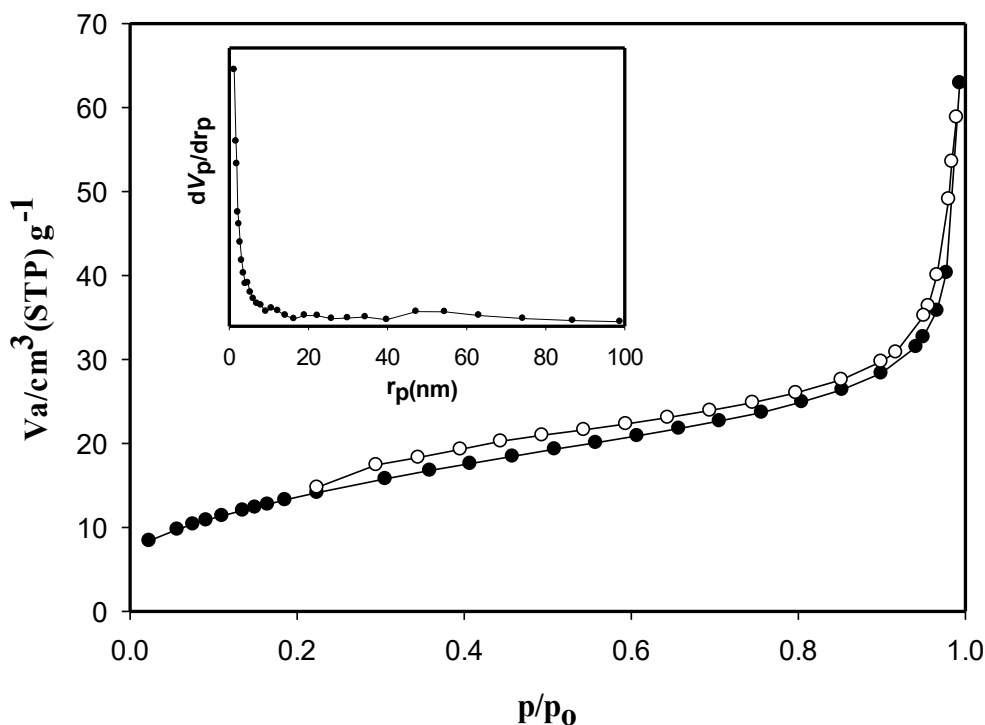
Fig. 6. N$_2$-adsorption-desorption of BTZ.

considering the isotropic nature of the crystal, where the material properties are independent of the direction along which they are measured. The uniform deformation model for BTZ nanoparticles is shown in Fig. 5.

The N$_2$ adsorption–desorption isotherms of BTZ sample is shown in Fig. 6. In accordance with the IUPAC nomenclature, both samples show typical IV type isotherms and H$_1$ type hysteresis looped at high relative pressures [26]. It can be seen from Fig. 1, that all adsorption and desorption isotherms display a sharp rise at medium relative pressure P/P$_0$ of 0.2–0.8.

The SEM image of BTZ (Fig. 7) shows smooth shericals and well-defined edges. The average particle size of these BTZ powders is about 50 nm and exhibits homogeneous distribution of the size and shape. The size distribution is shown in Fig. 6e. The maximum frequency of the particles' size is under 50 nm.

Fig. 8 shows thermal stabilities of BTZ determined by thermogravimetric analysis in the range of 25–1000 °C. The 3.72 % mass loss of BTZ in the temperature range of 25–150 °C is attributed to was attributed to dehydration reactions. A smooth weight loss step of over 10.21 % was also observed as the temperature increased from 250 to 700 °C, which occurs due to the combustion/oxidation of BTZ reactions in that temperature range [27]. Approximately 86.07 % of the starting weight remained after the decomposition, which indicates the formation of the metal oxides.

To further investigate the acidity sites of BTZ, we carried out the temperature-programmed desorption of NH$_3$-TPD (Fig. 9) which explains three peaks. Two peaks at around 231 and 870 °C implies the weak range acidic sites and another peak at around 528 °C displays the strong acidic sites. These strong acidic sites are disclosed due to Lewis acidity of ZrO$_2$ nanoparticles [28].

Synthesis of 1,5-benzodiazepine derivatives

The best experimental procedure was obtained via optimization of the catalytic amount of BTZ, various solvents and reaction temperature (Table 2). The optimal conditions have been established with 0.05 g of BTZ in CH$_3$CN under reflux condition.

The synthesis of 2,3-dihudro-1H-1,5-benzodiazepines by the condensation of 1,2-phenylenediamine with ketones catalyzed by BTZ in acetonitrile and under reflux conditions within 10 min in 85–98% yield. It is noteworthy to
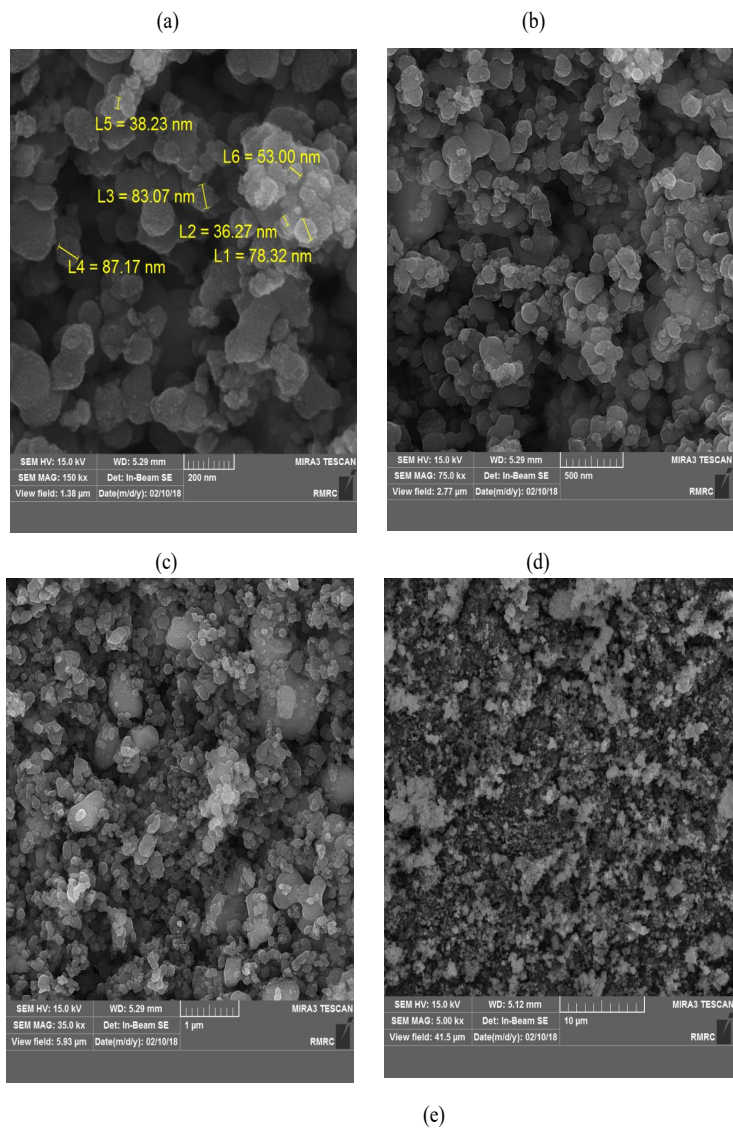
(a)

(b)

(c)

(d)

(e)

Fig. 7. (a-d) FE-SEM images and (e) size distribution (based on SEM analysis) of BTZ.
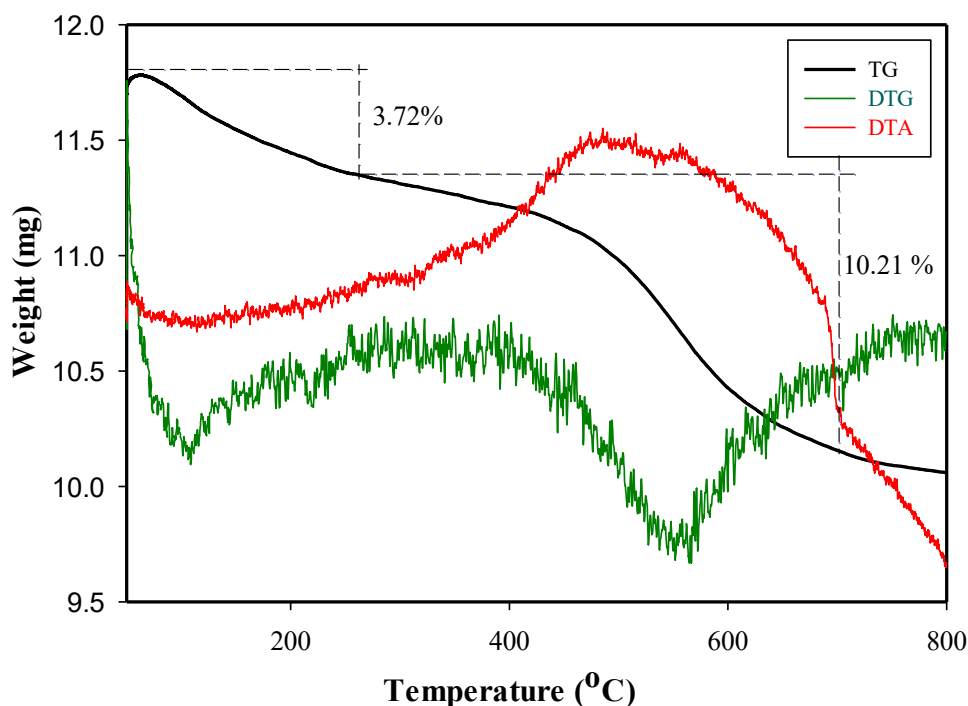
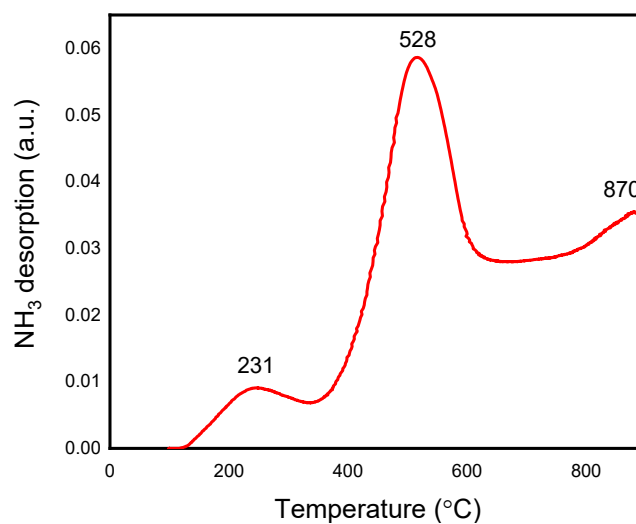Fig. 8. (a) TG (b) DTG and (c) DTA analysis of BTZ.

Fig. 9. NH$_3$-TPD analysis of BTZ.

mention that by starting from an unsymmetrical ketone, such as 2-butanone (Table 3, entry c), the ring closure occurs selectively only from one side of carbonyl group yielding a single product. Cyclic ketones, such as cyclopentanone and cyclohexanone (Table 3, entries e,f) also reacted
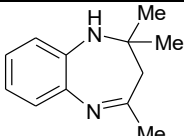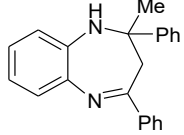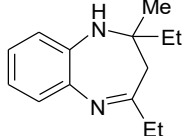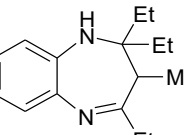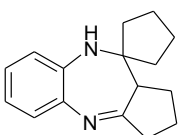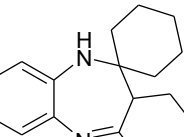
effectively to produce the corresponding fused ring benzodiazepines in CH$_3$CN or in the absence of solvent.

A reasonable pathway for the reaction of diamine with ketone in the presence of supported BTZ is also presented by Fig. 10.

Table 2. Effect of catalysts under different reaction conditions for condensation of 1,2-phenylenediamine and acetone after 30 min.

Entry	Catalyst	Temperature (°C)	solvent	Yield (%)[a]
1	-	Reflux	CH_3CN	0
2	$BaTiO_3$ (0.05 g)	Reflux	CH_3CN	45
3	$BaTi_{0.85}Zr_{0.15}O_3$ (0.03 g)	Reflux	CH_3CN	75
4	$BaTi_{0.85}Zr_{0.15}O_3$ (0.05 g)	Solvent-free	CH_3CN	98
5	$BaTi_{0.85}Zr_{0.15}O_3$ (0.07 g)	Reflux	CH_3CN	98
6	$BaTi_{0.85}Zr_{0.15}O_3$ (0.05 g)	Reflux	H_2O	65
7	$BaTi_{0.85}Zr_{0.15}O_3$ (0.05 g)	Reflux	CH_3OH	72
8	$BaTi_{0.85}Zr_{0.15}O_3$ (0.05 g)	Reflux	C_2H_5OH	75
9	$BaTi_{0.85}Zr_{0.15}O_3$ (0.05 g)	Reflux	CH_2Cl_2	48
10	$BaTi_{0.85}Zr_{0.15}O_3$ (0.05 g)	r.t.	CH_3CN	70

[a] Isolated yield.

Table 3. $BaTi_{0.85}Zr_{0.15}O_3$ -catalyzed formation of 2,3-dihydro-1H-1,5-benzodiazepines after 10 min.

Ketone	Product	Yield (%)[a]	Melting point Found	Report [6]
Acetone		98	141	137-139
Acetophenone		92	152	151-152
2-Butanone		98	138	137-138
3-Pentanone		95	138	144-145
Cyclopentanone		90	138	138-139
Cyclohexanone		85	139	137-139

itions: diamine (1 mmol), ketone (2.5 mmol), $BaTi_{0.85}Zr_{0.15}O_3$ (0.05 g), Solvent-free.
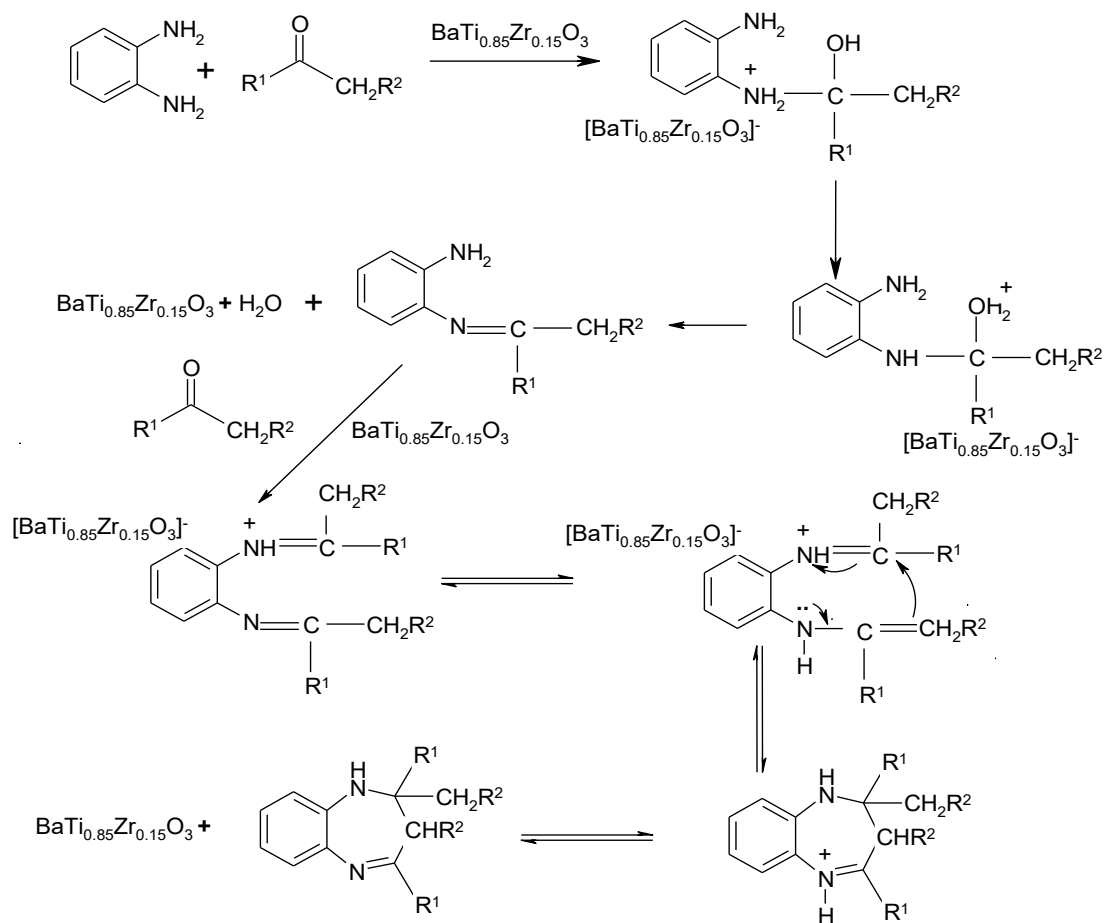yields after column chromatography.

Fig. 10. Proposed mechanism for the synthesis of 1,5-benzodiazepine derivatives by $BaTi_{0.85}Zr_{0.15}O_3$ (BTZ).
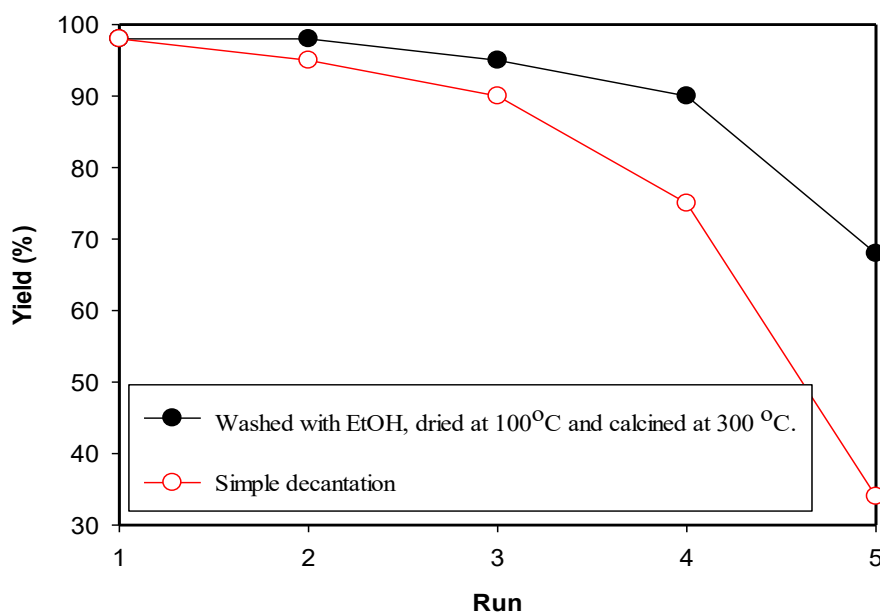

Fig. 11. The reusability study after third reaction cycles for BTZ catalyst.

The recovery and reusability of the supported catalysts have been investigated. We have noticed that after the addition of ETOH to the reaction mixture, BTZ can be easily recovered quantitatively by simple filtration. The wet catalyst was recycled (the nature of the recovered catalysts has been followed by NAA, XRD and FTIR spectra), but no appreciable change in the catalytic activity was observed up to four cycles if calcination of reused catalyst was occurred (Fig. 11).

CONCLUSION

In summary, novel and efficient BTZ was prepared under hydrothermal conditions and characterized by FTIR, XRD, SEM, BET, and TGA, and NH_3-TPD analysis. The catalytic activity of BTZ was investigated for synthesis of 1,5-benzodiazepine derivatives by reaction of o-phenylenediamine with different ketones. The significant advantages of this procedure are short reaction times, high yields, mild reaction conditions and reusability of catalyst for several times.

CONFLICT OF INTEREST

The authors declare that there is no conflict of interests regarding the publication of this manuscript.

ACKNOWLEDGEMENTS

REFERENCES

1. Garg M, Chawla M, Chunduri V, Kumar R, Sharma S, Sharma NK, et al. Transfer of grain colors to elite wheat cultivars and their characterization. Journal of Cereal Science. 2016;71:138-144.
2. The Benzodiazepines Edited by S. Garattini, E. Mussini, and L. O. Randall. (Pp. 685; illustrated; $35·00.) Raven Press: New York. 1973. Psychological Medicine. 1974;4(3):346-346.
3. Fazaeli R, Aliyan H, Tangestaninejad S. Aluminum Dodecatungstophosphate Promoted Synthesis of 1,5-Benzodiazepine Derivatives under Solvent-Free Conditions. HETEROCYCLES. 2007;71(4):805.
4. Zhang HN, Chen XH, Wang QP, Zhang XY, Chang J, Gao L, et al. High-efficiency diode-pumped actively Q-switched ceramic Nd:YAG/BaWO$_4$ Raman laser operating at 1666 nm. Optics Letters. 2014;39(9):2649.
5. Zhou X, Zhang MY, Gao ST, Ma JJ, Wang C, Liu C. An efficient synthesis of 1,5-benzodiazepine derivatives catalyzed by boric acid. Chinese Chemical Letters. 2009;20(8):905-908.
6. Fazaeli R, Aliyan H. Clay (KSF and K10)-supported heteropoly acids: Friendly, efficient, reusable and heterogeneous catalysts for high yield synthesis of 1,5-benzodiazepine derivatives both in solution and under solvent-free conditions. Applied Catalysis A: General. 2007;331:78-83.
7. Radatz CS, Silva RB, Perin G, Lenardão EJ, Jacob RG, Alves D. Catalyst-free synthesis of benzodiazepines and benzimidazoles using glycerol as recyclable solvent. Tetrahedron Letters. 2011;52(32):4132-4136.
8. Prakash GKS, Paknia F, Narayan A, Mathew T, Olah GA. Synthesis of perimidine and 1,5-benzodiazepine derivatives using tamed Brønsted acid, BF$_3$–H$_2$O. Journal of Fluorine Chemistry. 2013;152:99-105.
9. Karimi-Maleh H, Ayati A, Ghanbari S, Orooji Y, Tanhaei B, Karimi F, et al. Recent advances in removal techniques of Cr(VI) toxic ion from aqueous solution: A comprehensive review. Journal of Molecular Liquids. 2021;329:115062.
10. Karimi-Maleh H, Karimi F, Orooji Y, Mansouri G, Razmjou A, Aygun A, et al. A new nickel-based co-crystal complex electrocatalyst amplified by NiO dope Pt nanostructure hybrid; a highly sensitive approach for determination of cysteamine in the presence of serotonin. Scientific Reports. 2020;10(1).
11. Karimi-Maleh H, Karimi F, Malekmohammadi S, Zakariae N, Esmaeili R, Rostamnia S, et al. An amplified voltammetric sensor based on platinum nanoparticle/polyoxometalate/two-dimensional hexagonal boron nitride nanosheets composite and ionic liquid for determination of N-hydroxysuccinimide in water samples. Journal of Molecular Liquids. 2020;310:113185.
12. Karimi-Maleh H, Ranjbari S, Tanhaei B, Ayati A, Orooji Y, Alizadeh M, et al. Novel 1-butyl-3-methylimidazolium bromide impregnated chitosan hydrogel beads nanostructure as an efficient nanobio-adsorbent for cationic dye removal: Kinetic study. Environmental Research. 2021;195:110809.
13. Karimi-Maleh H, Alizadeh M, Orooji Y, Karimi F, Baghayeri M, Rouhi J, et al. Guanine-Based DNA Biosensor Amplified with Pt/SWCNTs Nanocomposite as Analytical Tool for Nanomolar Determination of Daunorubicin as an Anticancer Drug: A Docking/Experimental Investigation. Industrial & Engineering Chemistry Research. 2021;60(2):816-823.
14. Haertling GH. Ferroelectric Ceramics: History and Technology. Journal of the American Ceramic Society. 1999;82(4):797-818.
15. Shrout TR, Zhang S. Lead-free piezoelectric ceramics: Alternatives for PZT? Journal of Electroceramics. 2007;19(1):185-185.
16. Karaki T, Yan K, Miyamoto T, Adachi M. Lead-Free Piezoelectric Ceramics with Large Dielectric and Piezoelectric Constants Manufactured from BaTiO$_3$ Nano-Powder. Japanese Journal of Applied Physics. 2007;46(No. 4):L97-L98.
17. Hennings D, Schnell A, Simon G. Diffuse Ferroelectric Phase Transitions in Ba(Ti$_{1-y}$Zr$_y$)O$_3$ Ceramics. Journal of the American Ceramic Society. 1982;65(11):539-544.
18. Stojanovic BD, Simoes AZ, Paiva-Santos CO, Jovalekic C, Mitic VV, Varela JA. Mechanochemical synthesis of barium titanate. Journal of the European Ceramic Society. 2005;25(12):1985-1989.
19. Cernea M, Monnereau O, Llewellyn P, Tortet L, Galassi C. Sol–gel synthesis and characterization of Ce doped-BaTiO3. Journal of the European Ceramic Society. 2006;26(15):3241-3246.
20. Keshri S, Joshi L, Rout SK. Influence of BTO phase on

structural, magnetic and electrical properties of LCMO. Journal of Alloys and Compounds. 2009;485(1-2):501-506.

21. Dobal PS, Dixit A, Katiyar RS, Yu Z, Guo R, Bhalla AS. Micro-Raman scattering and dielectric investigations of phase transition behavior in the $BaTiO_3$–$BaZrO_3$ system. Journal of Applied Physics. 2001;89(12):8085-8091.

22. Alexander L, Klug HP. Determination of Crystallite Size with the X-Ray Spectrometer. Journal of Applied Physics. 1950;21(2):137-142.

23. Aliyan H, Fazaeli R. Pd/APN-Mn(BTC) as novel, highly efficient, and recyclable catalyst for Suzuki–Miyaura cross coupling reaction. Canadian Journal of Chemistry. 2020;98(8):445-452.

24. Lili L, Xin Z, Shumin R, Ying Y, Xiaoping D, Jinsen G, et al. Catalysis by metal–organic frameworks: proline and gold functionalized MOFs for the aldol and three-component coupling reactions. RSC Adv. 2014;4(25):13093-13107.

25. Tagliente MA, Massaro M. Strain-driven (002) preferred orientation of ZnO nanoparticles in ion-implanted silica. Nuclear Instruments and Methods in Physics Research Section B: Beam Interactions with Materials and Atoms. 2008;266(7):1055-1061.

26. Liu Q, Low Z-X, Li L, Razmjou A, Wang K, Yao J, et al. ZIF-8/Zn_2GeO_4 nanorods with an enhanced CO_2 adsorption property in an aqueous medium for photocatalytic synthesis of liquid fuel. Journal of Materials Chemistry A. 2013;1(38):11563.

27. Antonelli E, Silva RS, Hernandes AC. $Ba(Ti_{1-x}Zr_x)O_3$(x = 0,05 and 0,08) Ceramics Obtained from Nanometric Powders: Ferroelectric and Dielectric Properties. Ferroelectrics. 2006;334(1):75-82.

28. Watanabe M, Aizawa Y, Iida T, Nishimura R, Inomata H. Catalytic glucose and fructose conversions with TiO_2 and ZrO_2 in water at 473K: Relationship between reactivity and acid–base property determined by TPD measurement. Applied Catalysis A: General. 2005;295(2):150-156.